

CHAPTER 4

COMPUTER MODELING

4.1 Introduction

In this chapter, the underlying concepts related to the computer modeling of the flow around bridges are discussed. The issues related to solving the equations of structure and fluid numerically are explained with reference to the Fluid Structure Interaction. The solution procedures and the pertinent equations for the fluid and the structure are stated and enunciated. The relevant boundary and initial conditions and the advantages of the solution procedures adopted are also studied.

4.2 The Structure

The structure used in this work is the Great Belt East Bridge(GBEB) girder section. The GBEB is a 3 span box girder suspension bridge of span lengths 535m-1624m-535m, which carries a four-lane motorway across the international shipping route of the Great Belt, Denmark (Larsen et. al. 1999). The design of the bridge was initiated in 1989 and opened to traffic in 1998 after construction. Two different cross-sections were used for the approach and the suspension spans as shown in Figures 4.2 and 4.3. From Figure 4.1, it can be seen that the center of gravity for the suspension section is different from the shear center and lies above the shear center. This is worth noting in the sense that the section rotates about the shear center due to the moment, whereas the translational displacement occurs about the center of gravity. Since both are located along the line of symmetry, there is no coupling of the rotational and translational

displacements. Tacoma's Narrows bridge is also shown here as a comparison against the GBEB bridge section.

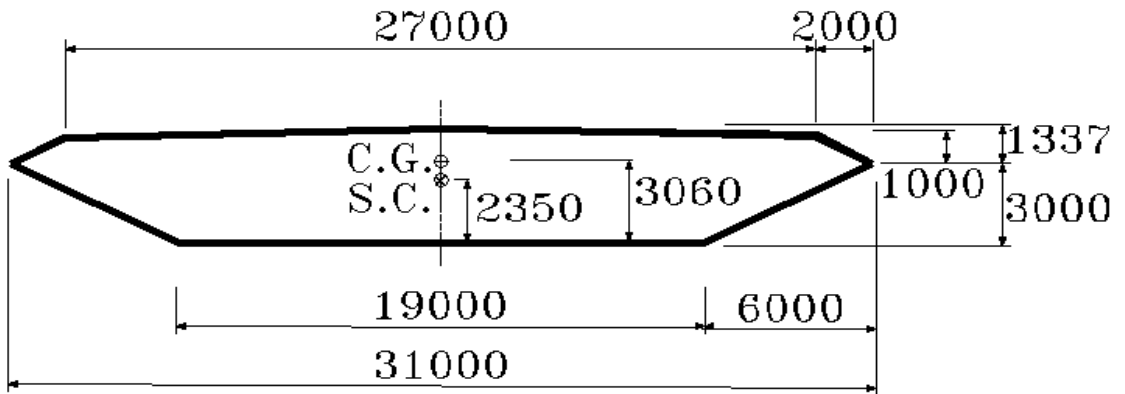


Figure 4.1 Cross-section of the Great Belt East Bridge (GBEB) suspension span.
(All dimensions are in mm). Picture from Walther, 1994.

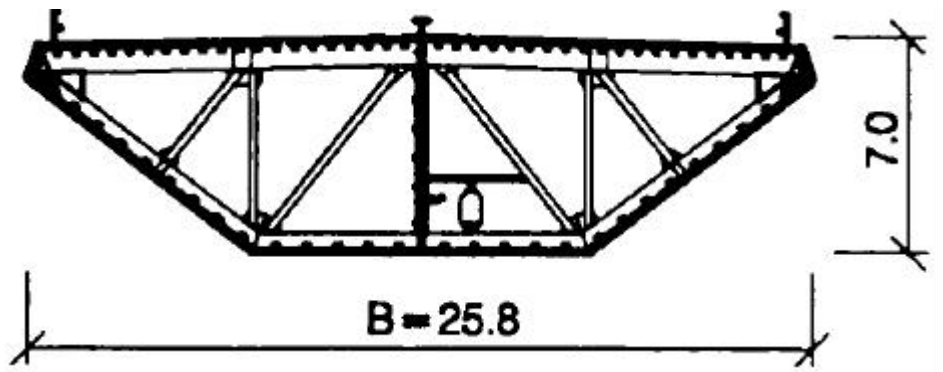


Figure 4.2 Great Belt East Bridge girder - Approach span

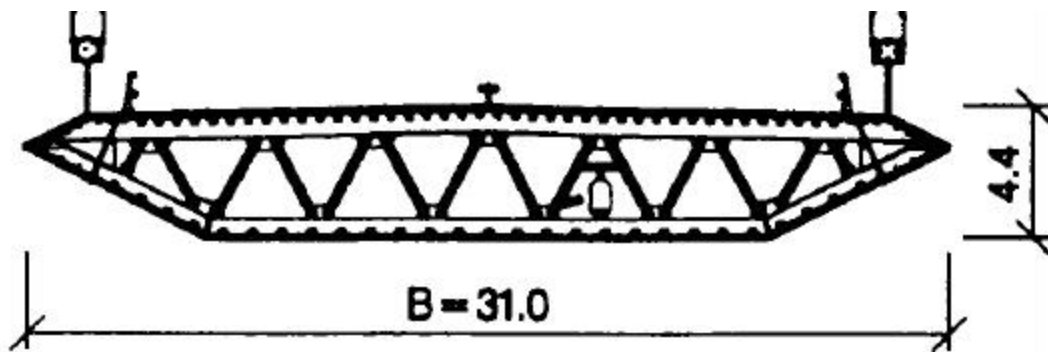


Figure 4.3 Great Belt East Bridge girder - Suspension span

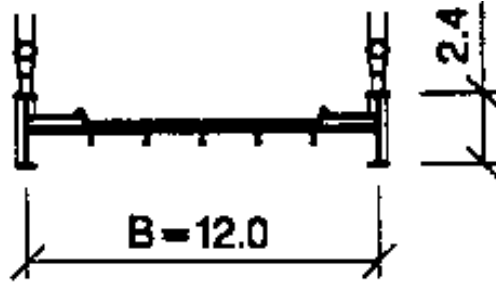


Figure 4.4 1st Tacoma Narrows Bridge

(The pictures of bridge cross-sections are from Larsen and Walther, 1996)

Structural property	Mass(Kg/m)	Inertia(Kgm ² /m)	f _h (Hz)	f _a (Hz)
GBEB Suspension	22.7*10 ³	2.47*10 ⁶	0.099	0.272
GBEB Approach	16.0*10 ³	1.05*10 ⁶	0.46	2.76
1 st Tacoma Narrows	1.3*10 ³	28.19*10 ³	0.13	0.20

Table 4.1. Structural properties of bridge cross sections (Larsen 1996).

4.3 Flow Parameters

The flow is characterized by parameters like Reynolds number, Strouhal number, coefficient of drag force, lift force and moment. They are defined as follows.

$$R_e = \frac{VB}{u} \quad 4.1$$

$$C_d = \frac{F_x}{0.5rV^2BW}$$

$$C_l = \frac{F_y}{0.5rV^2BW}$$

$$C_m = \frac{M}{0.5rV^2B^2W}$$

$$S_t = \frac{H}{TV}$$

Where

B, H, W —————► width, height, length in the z direction of the bridge respectively

F_x, F_y —————► drag and lift forces

V —————► reference velocity,

\mathbf{u} —————► kinematic viscosity,

M —————► moment

T —————► period of oscillation of the lift forces

\mathbf{r} —————► density.

For 2D computation, W is considered to be one.

4.4 Governing Equations for Flow

In the modeling, the fluid is assumed to be viscous and incompressible and the Navier Stokes equations are used to study and describe the fluid flow around the bridge girder. The governing Navier Stokes equations in two and three-dimensions for an incompressible fluid using the Large Eddy Simulation (LES) model in general tensor notation, as reported by Selvam (2000) are as follows.

$$\text{Continuity Equation: } U_{i,i} = 0 \quad 4.2$$

$$\text{Momentum Equation: } U_{i,t} + (U_j - V_j)U_{i,j} = -\left(\frac{p}{\mathbf{r}} + \frac{2k}{3}\right)_{,i} + [(\mathbf{u} + \mathbf{u}_t)(U_{i,j} + U_{j,i})]_{,j} \quad 4.3$$

where

$$\mathbf{u}_t = (C_s h)^2 \sqrt{S_{ij}^2 / 2},$$

$$S_{ij} = U_{i,j} + U_{j,i},$$

$$h = \sqrt[3]{h_1 h_2 h_3} \text{ for 3D}$$

$$h = \sqrt{h_1 h_2} \text{ for 2D}$$

$$k = \left(\frac{\mathbf{u}_t}{C_k h} \right)^2$$

Empirical constants $C_s=0.15$ for 2D and 0.1 for 3D and $C_k=0.094$

Here

U_i —————► mean velocity

p —————► pressure

V_i —————► grid velocity

k —————► turbulent kinetic energy

\mathbf{u}_t —————► turbulent eddy viscosity

\mathbf{r} —————► fluid density

h_1, h_2 and h_3 —————► control volume spacing in the x, y, z directions

For the computation of h , the area is used if it is a two-dimensional model or the volume is used if the model is three-dimensional. Here a comma represents differentiation, t represents time and $i=1, 2$ and 3 mean variables in the x, y and z directions. Selvam (2000,1998b) reports that to implement higher order approximation of the convection term the following expression is used in Equation 4.3 instead of $U_j U_{i,j}$

$$(U_j - V_j)U_{i,j} - \mathbf{q}[(U_j - V_j)(U_k - V_k)U_{i,j}]_{,k} / 2 \tag{4.4}$$

He states that depending upon the values of q , different procedures can be implemented. For balance tensor diffusivity (BTD) scheme, $q = dt$ is used; where dt is the time step used in the integration. For streamline upwind procedure suggested, q is considered as:

$$q = 1/\max (|U_1|/dx, |U_2|/dy, |U_3|/dz) \quad 4.5$$

Here

dx, dy and dz —————► control volume length

U_1, U_2 and U_3 —————► velocities in the x, y and z directions

In this computation $q = dt$ is used. This has less numerical diffusion as compared to benchmark problems in Selvam (1998). For moving grid the maximum of the BTD or 0.3 times equation 4.5 is considered for better stability of the solution.

4.5 Governing Equations for Structure

When the wind flows over the structure, the structure is subjected to both translation (vertical) and rotational (twisting) motion. Figure 4.5 shows the GBEB section with both the vertical and rotating degrees of freedom. The differential equations describing both these types of motion are as follows. The equations are non-dimensionalised with respect to the dimension B and then solved in a non-dimensional form. The non-dimensionalised representation of time(t), vertical displacement(y), angular displacement(a) and velocity(V) are as shown below. The asterisk represents the non-dimensional value.

$$t^* = \frac{tV_\infty}{B} \quad ; \quad y^* = \frac{y}{B} \quad ; \quad a^* = a \quad ; \quad u^* = \frac{V_\infty}{wB}$$

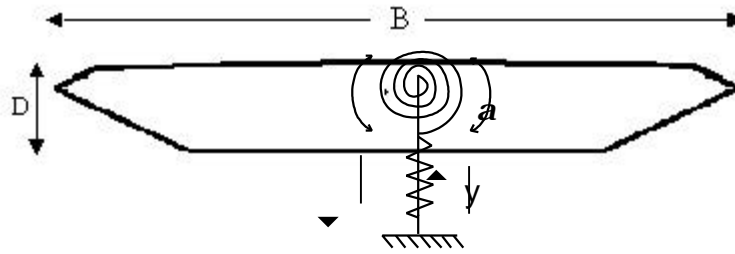


Fig 4.5 Structural model of the GBEB section.

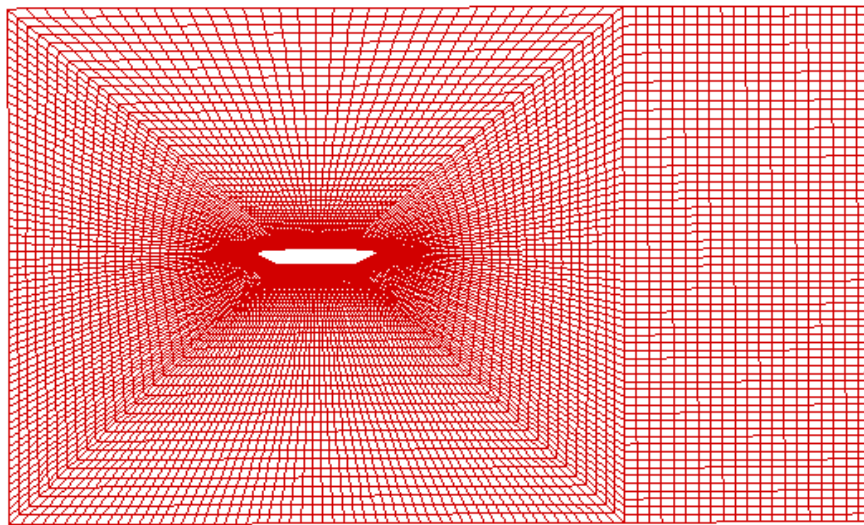


Fig 4.6 The FEM grid system of the suspension span of the GBEB section.

4.5.1 Translation motion

The differential equation for the translatory motion is given by

$$m\ddot{y} + K_h y = F_l(t) \tag{4.6}$$

where F_l \longrightarrow Lift force as described in section 4.3

K_h \longrightarrow vertical stiffness

y \longrightarrow vertical displacement

\ddot{y} \longrightarrow vertical acceleration

m \longrightarrow mass

Rewriting equation (4.6) gives

$$\ddot{y} + \mathbf{w}_h^2 y = \frac{F_l(t)}{m} \quad \text{where } \mathbf{w}_h^2 \longrightarrow \frac{K_h}{m} \quad 4.7$$

Non-dimensionalising each of the terms in the above equation, we get

$$\dot{y} = \frac{dy}{dt} = \frac{d(By^*)}{d\left(\frac{t^* B}{V_\infty}\right)} \quad \text{where } y = By^* \text{ and } t = \frac{t^* B}{V_\infty}$$

The second derivative becomes

$$\ddot{y} = \frac{d^2 y}{dt^2} = \frac{d^2 (By^*)}{d\left(\frac{t^* B}{V_\infty}\right)^2} = \frac{V_\infty^2}{B} \frac{d^2 y^*}{dt^{*2}}$$

Now substituting the non-dimensional terms \ddot{y} and \dot{y} and rewriting equation 4.7 in non-dimensional terms, we get

$$\frac{V_\infty^2}{B} \ddot{y}^* + \mathbf{w}_h^2 By^* = \frac{F_l(t)}{m} \quad 4.8$$

Multiplying both sides of (4.8) by $\frac{B}{V_\infty^2}$ gives

$$\ddot{y}^* + \mathbf{w}_h^2 \frac{B^2}{V_\infty^2} y^* = \frac{F_l(t)}{m} \frac{B}{V_\infty^2} \quad 4.9$$

Now including the lift force, $F_l(t) = 0.5C_l \mathbf{r} V_\infty^2 B$ and non-dimensional form of velocity $V_\infty = u^* \mathbf{w}_h B$ into 4.9, we get the final dynamic equation for translation in the non-dimensional form as follows.

$$\ddot{y}^* + \left(\frac{w_h}{w_a}\right)^2 \left(\frac{1}{u^*}\right)^2 y^* = \frac{C_l}{2R_m} \quad \text{where } R_m = \frac{m}{rB^2} \quad 4.10$$

4.5.2 Rotational Motion

The differential equation for rotational motion is given by

$$I_a \ddot{\mathbf{a}} + K_a \mathbf{a} = M_a(t) \quad 4.11$$

where I_a —————► Mass moment of inertia

\mathbf{a} —————► Angular displacement

$\ddot{\mathbf{a}}$ —————► Angular acceleration

K_a —————► Rotational stiffness

$M_a(t)$ —————► Force due to moment

Proceeding in the same manner as previously, rewriting equation (4.11) gives

$$\ddot{\mathbf{a}} + w_a^2 \mathbf{a} = \frac{M_a(t)}{I} \quad \text{where } w_a^2 \longrightarrow \frac{K_a}{I_a} \quad 4.12$$

Non-dimensionalising each of the terms in the above equation, we get

$$\dot{\mathbf{a}} = \frac{d\mathbf{a}}{dt} = \frac{d(\mathbf{a}^*)}{d\left(\frac{t^* B}{V_\infty}\right)} \quad \text{where } \mathbf{a} = \mathbf{a}^* \text{ and } t = \frac{t^* B}{V_\infty}$$

The second derivative becomes

$$\ddot{\mathbf{a}} = \frac{d^2 \mathbf{a}}{dt^2} = \frac{d^2 (B \mathbf{a}^*)}{d\left(\frac{t^* B}{V_\infty}\right)^2} = \frac{V_\infty^2}{B^2} \frac{d^2 \mathbf{a}^*}{dt^{*2}}$$

Now substituting the non-dimensional terms $\ddot{\mathbf{a}}$, $\dot{\mathbf{a}}$ and rewriting equation 4.12 in non-dimensional terms, we get

$$\frac{V_{\infty}^2}{B^2} \ddot{\mathbf{a}} + \mathbf{w}_a^2 \mathbf{a}^* = \frac{M_a(t)}{I_a} \quad 4.13$$

Multiplying both sides of (4.13) by $\frac{B^2}{V_{\infty}^2}$ gives

$$\ddot{\mathbf{a}}^* + \mathbf{w}_a^2 \frac{B^2}{V_{\infty}^2} \mathbf{a}^* = \frac{M_a(t)}{I_a} \frac{B^2}{V_{\infty}^2} \quad 4.14$$

Now including the lift force, $M_a(t) = 0.5C_m \mathbf{r} V_{\infty}^2 B^2$ and non-dimensional form of velocity $V_{\infty} = u^* \mathbf{w}_a B$ into 4.14, we get the final dynamic equation for rotation in the non-dimensional form as follows.

$$\ddot{\mathbf{a}}^* + \left(\frac{1}{u^*} \right)^2 \mathbf{a}^* = \frac{C_m}{2R_l} \quad \text{where } R_l = \frac{I_a}{\mathbf{r} B^4} \quad 4.15$$

The ratio of the frequency of heave and pitch oscillation is a factor called *whp* that is used in the computations.

The parameters R_l , R_m and *whp* are calculated from the physical properties of the GBEB bridge girder for an air density of $\mathbf{r} = 1.228 \text{ kg/m}^3$ as given below.

$$R_l = \frac{I_a}{\mathbf{r} B^4} = 2.178$$

$$R_m = \frac{m}{\mathbf{r} B^2} = 19.236$$

$$\text{whp} = \frac{\mathbf{w}_h}{\mathbf{w}_a} = 0.364$$

4.6 Computational Grid

A structured body conforming grid was used for the GBEB bridge section in the simulation process. As mentioned in the grid generation chapter, several issues like variation of spacing, aspect ratio, alignment and size and shape of the elements, optimum number of elements is to be considered. Four different grids are generated keeping in mind the parameters like the total number of nodes, spacing close to the bridge deck and the concentration of density in flow separation regions. The finite element code was run using these four grids in order to assess the influence of the grid parameters on the results.

The grids A and B were generated by an in-house program developed by the author. In this program, each line segment of the bridge cross-section was divided into zones and the desired number of grid points in each of the zones was fed as an input in the data file. The spacing among the points in each zone is calculated by the series of geometric progression. At the intersection of the two line segments of the bridge cross-section, a smooth transition of the grid is ensured by merging the spacing of the previous zone into the start of a new zone. Within each zone the spacing is varied in an increasing or decreasing fashion according to the direction and nature of the flow occurring around that region of the cross-section. Controlling the common ratio in the geometric series of progression effects the desired rate of increase/decrease in the variation of spacing. Here, the common ratio is defined as the percentage increase or decrease from the previous value.

The other two grids, namely C and D, were developed using the software GRIDGEN (Version 9) developed by NASA Ames Research Center. This software is

sophisticated and has more options for the grid generation process. This offers the choice of several blending functions and grid point distribution functions. A lot of details are mentioned in the Gridgen user manual. It has solvers like elliptic PDE solver and algebraic solver that can be iteratively applied to the grid to smoothen it. With GRIDGEN, two highly refined grids, C and D with a spacing of 0.0033 and 0.00065 respectively was developed. The elliptic PDE solver was used to refine and smoothen the grid. The tanh grid point distribution function was used in spacing the grid points radially from the corner of the bridge section to the outer boundary of the fluid domain. The details of the grid types A, B, C and D are given in Table 5.2. The pictures of the grid used are shown in Figures 4.9 through 4.14.

Grid Type	Grid Points	Elements	Nodes	Spacing close to deck
A	216 x 57	13515	13280	0.002
B	216 x 63	14805	14570	0.001
C	302 x 65	20745	20424	0.0033
D	312 x 57	18807	18476	0.00065

Table 4.2 Specifications of the configuration of the various grid types used.

4.7 Boundary and Initial conditions

The computational domain and the boundary conditions used are illustrated in Fig 4.1 for the fixed grid as reported by Selvam and Govindaswamy (2000). They also state that the cylinder surface has no slip condition. The upstream boundary has uniform velocity of one in the x direction and zero in the y direction. At the outflow boundary the normal

gradient of the velocities are zero and the sides have slip boundaries. The computation is done for Re of 10^5 .

Figure 4.7 shows the schematic representation of the domain chosen for the problem and the boundary conditions applied in the computations.

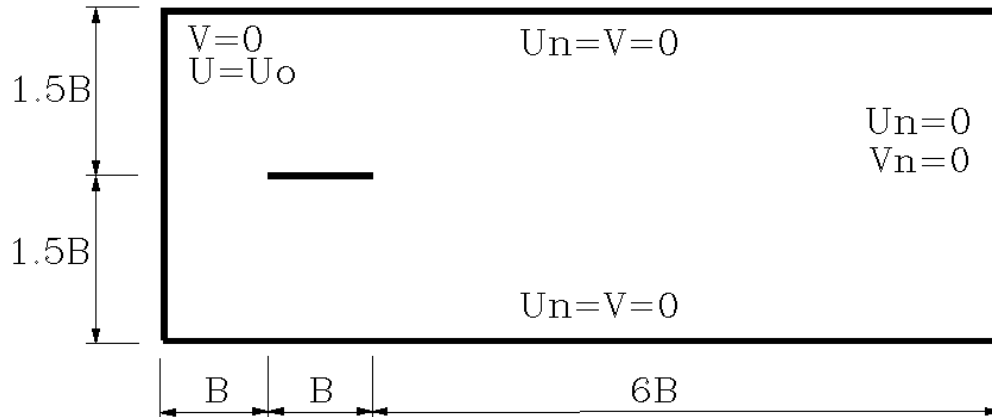


Fig 4.7 Solution domain and the Boundary conditions.

4.8 Finite Element Solution Procedure to solve the Fluid equations

The bridge section is subjected to the wind flow and the modeling is done as follows. The turbulence is modeled using Large Eddy Simulation (LES) and the governing equations are solved by Finite element method (FEM). The pressure on the bridge is computed by solving the Navier-Stokes equations and using this pressure the new position of the bridge is calculated by solving the structural mechanics equations. The flow is now solved over the new position of the structure and the grid is updated and the process is repeated for each time step. The time step size is calculated using a CFL (Courant-Frederick-Lewis) number less than one as reported by Selvam (1998). The Navier-Stokes equations are solved by Finite element procedure in a non-dimensional form. The

velocity and pressure are approximated using equal order interpolation. Eight noded brick element is used for 3D and four noded quadrilateral element is used for 2D.

The Navier-Stokes equations are solved using an implicit method suggested in Selvam (1998) in a four-step advancement scheme as follows:

Step 1: Solve for U_i from equation 5.3.

Step 2: Get new velocities as $U_i^* = U_i + \mathbf{dt}(p_{,i})$ where U_i is not specified

Step 3: Solve for pressure from $(p_{,i})_{,i} = U_{i,i}^* / \mathbf{dt}$

Step 4: Correct the velocity for incompressibility: $U_i = U_i^* - \mathbf{dt}(p_{,i})$ where U_i is not specified

In step 1, the diffusion and higher order convection terms are considered implicitly to be in the current time and the first order convection terms are considered explicitly from the previous time step. Implicit treatment of the convective and diffusive terms eliminates the numerical stability restrictions. The pressure is considered in the right hand side of the equation. This set of equations leads to a symmetric matrix and the preconditioned conjugate gradient (PCG) procedure is used to solve. For simplicity here on $\frac{p}{\mathbf{r}}$ is considered as p . Step 2 eliminates the checkerboard pressure field created when using equal order interpolation for velocity and pressure in the case of FEM.

The equations are stored in a compact form as discussed in Selvam (1998). To solve the velocities an under-relaxation factor of 0.7 is used. The iteration is done until the absolute sum of the residue of the equation reduces to 1×10^{-7} times the number of nodes for each time step. Usually the pressure and momentum equations take about 50 and 10 iterations for PCG solution respectively as reported by Selvam and Govindaswamy (2000).

4.9 Finite Element Scheme to solve the equations for Structure

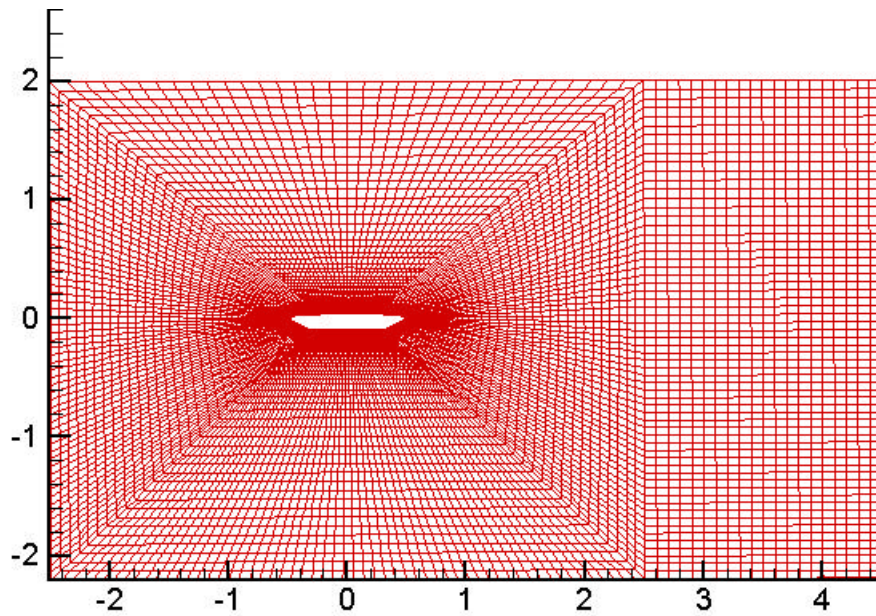
Once the Navier-Stokes equations are solved, the pressure and velocity from the flow is obtained. This calculated pressure is applied as a force over the bridge section. The force along the x direction is the drag force (C_d), in y direction it is the lift force (C_l) and the force inducing a rotation is the moment (C_m). The results of the solution of fluid equations, in terms of the lift (C_d) and moment (C_m) coefficients along with the values of the non-dimensional velocity (U^*), R_l , R_m and whp are fed into the equations of motion for structure as given by (4.10) and (4.15). The resultant displacement in the form of heave (h) and pitch (\mathbf{a}) is obtained by solving the non-dimensional form of the translatory and rotational equations of motion as given by 4.10 and 4.15 respectively. The bridge rotates about the shear center and moves vertically from the center of gravity. Since both these displacements occur along the line of symmetry, there is no coupling. The structural dynamics equations are solved in time explicitly using the central difference integration scheme. A constant time step size of 0.001 is used as against the variable time step size, used for the fixed computations. A time history of the data for these five variables, namely C_d, C_l, C_m, h , and \mathbf{a} are calculated and plotted.

4.10 Moving Grid

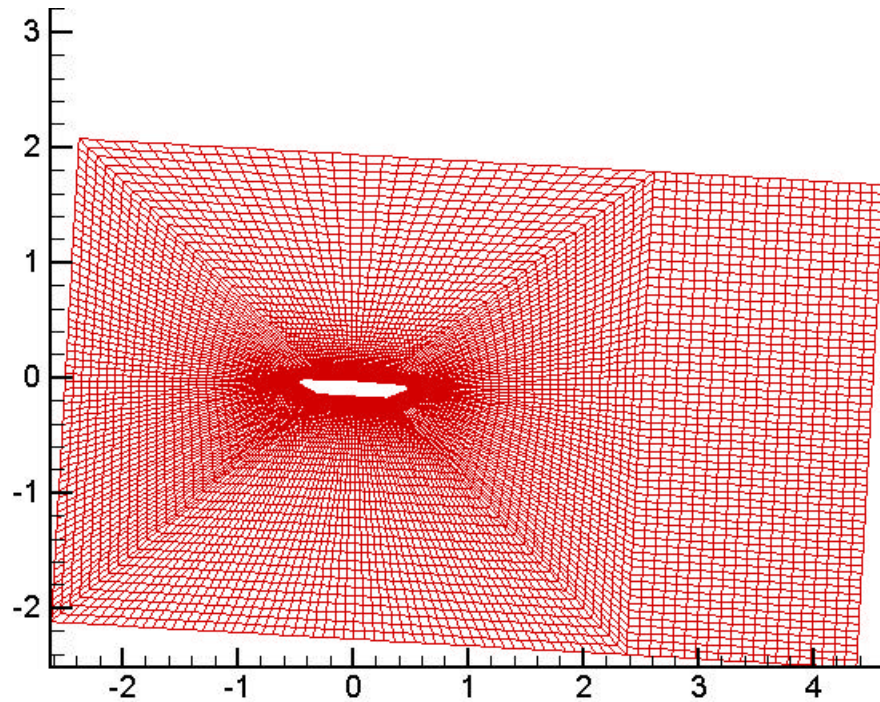
An arbitrary Lagrangian Eulerian (ALE) co-ordinate system is used for the description of both the structure and the fluid in the computational domain. Here the grid is moved according to the fluid structure interaction using the rigid body moving method. In this method, the grid is treated to be a rigid one during the flow and moved as a whole. The convective flux terms of the equations are modified in order to incorporate the

change in velocity of the moving elements. The correction is made by subtracting the velocity of the grid V_j from the velocity of the fluid U_j as shown by equation 4.4. The grid is treated as rigid and rotated as a whole about the shear center of the bridge section to match the corresponding structural deflections calculated during each time step. Thus the same grid is used for updating at each time in conformance with the flow.

The variables R_l, R_m, whp, U^* , and time step, as discussed in section 4.5 are given as input parameters in the moving bridge program and the response is plotted against time and the flutter velocity is calculated from these plots.



(a) Initial grid



(b) Displaced grid

Fig 4.8 (a)-(b) Movement of grid using the rigid body method.

4.11 Critical Flutter Velocity computation for Bridges

The critical velocity for bridges is calculated using the free oscillation procedure. In the Free motion of the bridge, the aeroelastic stability is observed directly. Here the cross-section is elastically suspended in the flow and the stability of the cross-section is observed for various wind speeds. In this procedure the bridge cross-section is given an initial perturbation of 1.8° and the subsequent displacements on the structure in-terms of heave and pitch is observed. The pressure is computed for the given position of the bridge by solving the Navier-Stokes equations. The force along x direction represents drag, the y direction represents lift, and the force that causes rotation represents moment. This pressure force is then applied at the center of gravity and the moment force is applied at the shear

center and the non-dimensional structural dynamic equations are solved. The solution gives the heave and pitch displacements. The grid is now updated by applying these displacements in a rigid body fashion. The grid velocity to be applied is the difference in the position from one time step to the next divided by the time step size. This process is continued for several times steps. The grid velocity is then incorporated in the Navier stokes equations (equation 4.4) to account for the movement of grid. The plot of the bridge position in time for various approach wind speeds gives the detail of the aeroelastic stability. The model is run for various non-dimensional velocities ranging from 0.4 to 1.5 to study the stability of the bridge during motion. This initial perturbation dies down to zero and stabilizes as time progresses, if the velocity is less than the critical flutter velocity. As the models are run with increasing velocities, the flutter velocity is reached and the initial perturbation gradually increases in time till it reaches catastrophic levels before it fails. The critical flutter velocity may be calculated in a few computer runs from the time history plots of the motion-induced response from the structure. This is explained in detail in the chapter 6.

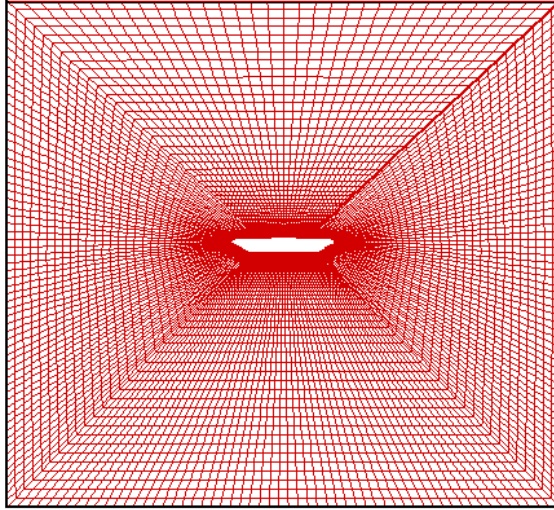


Fig 4.9 Grid-A

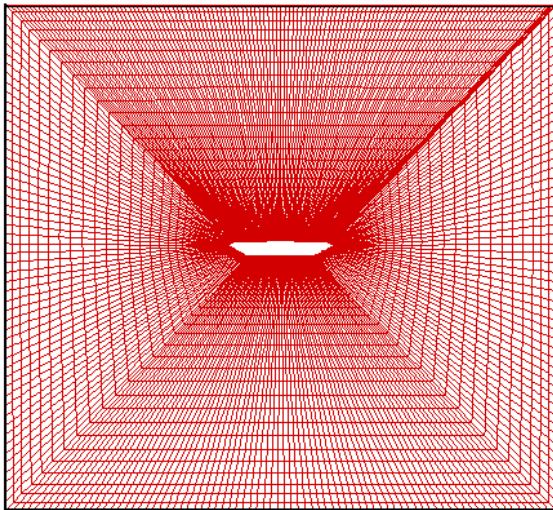


Fig 4.10 Grid-B

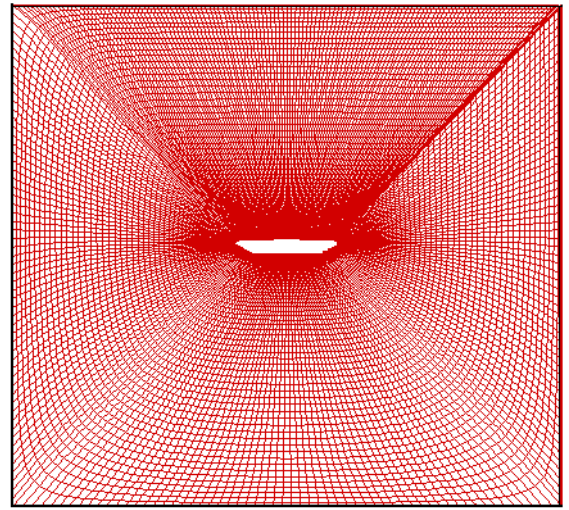


Fig 4.11 Grid-C

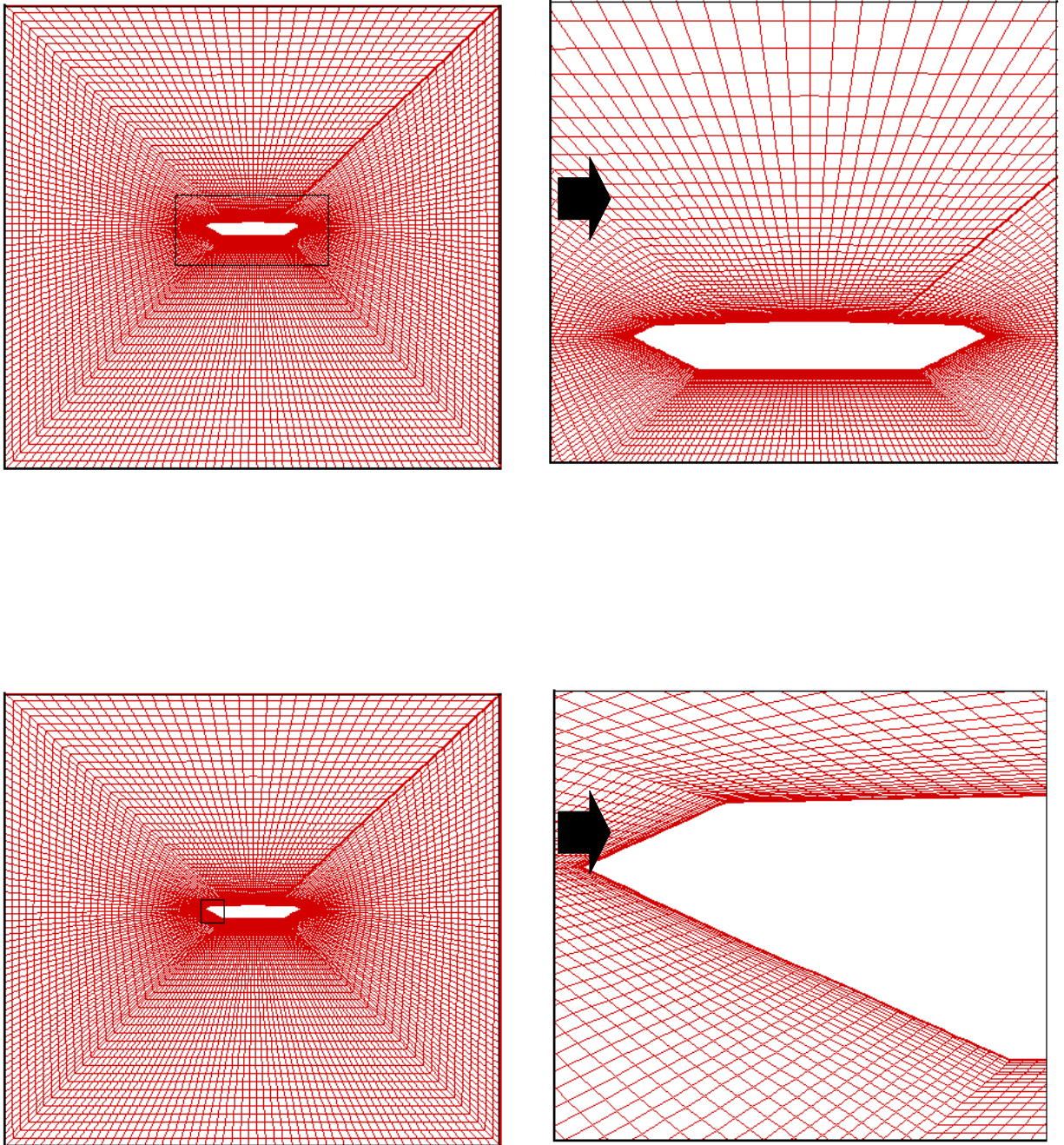


Fig 4.12 Close-up view of Grid-A

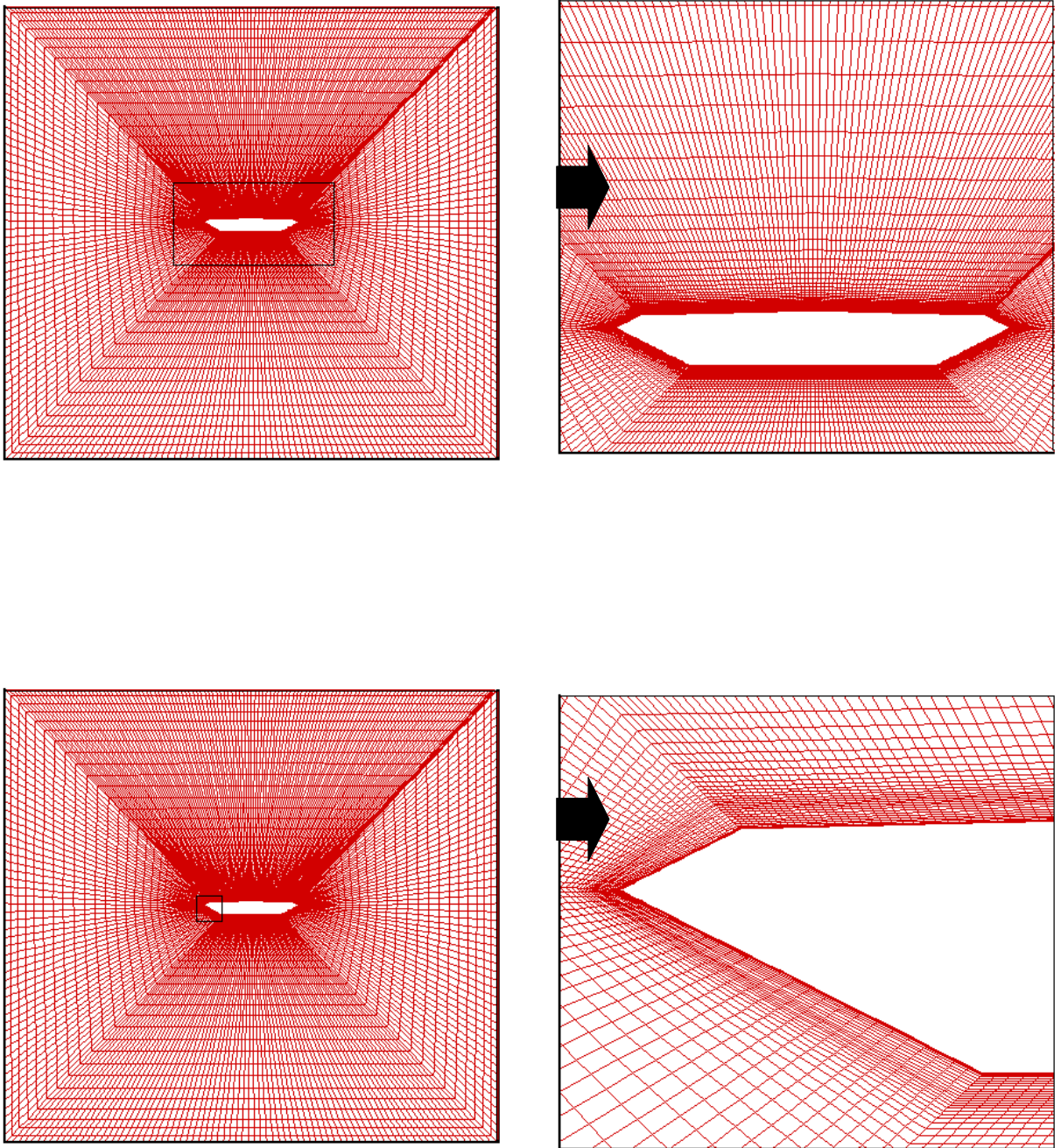


Fig 4.13 Close-up view of Grid-B

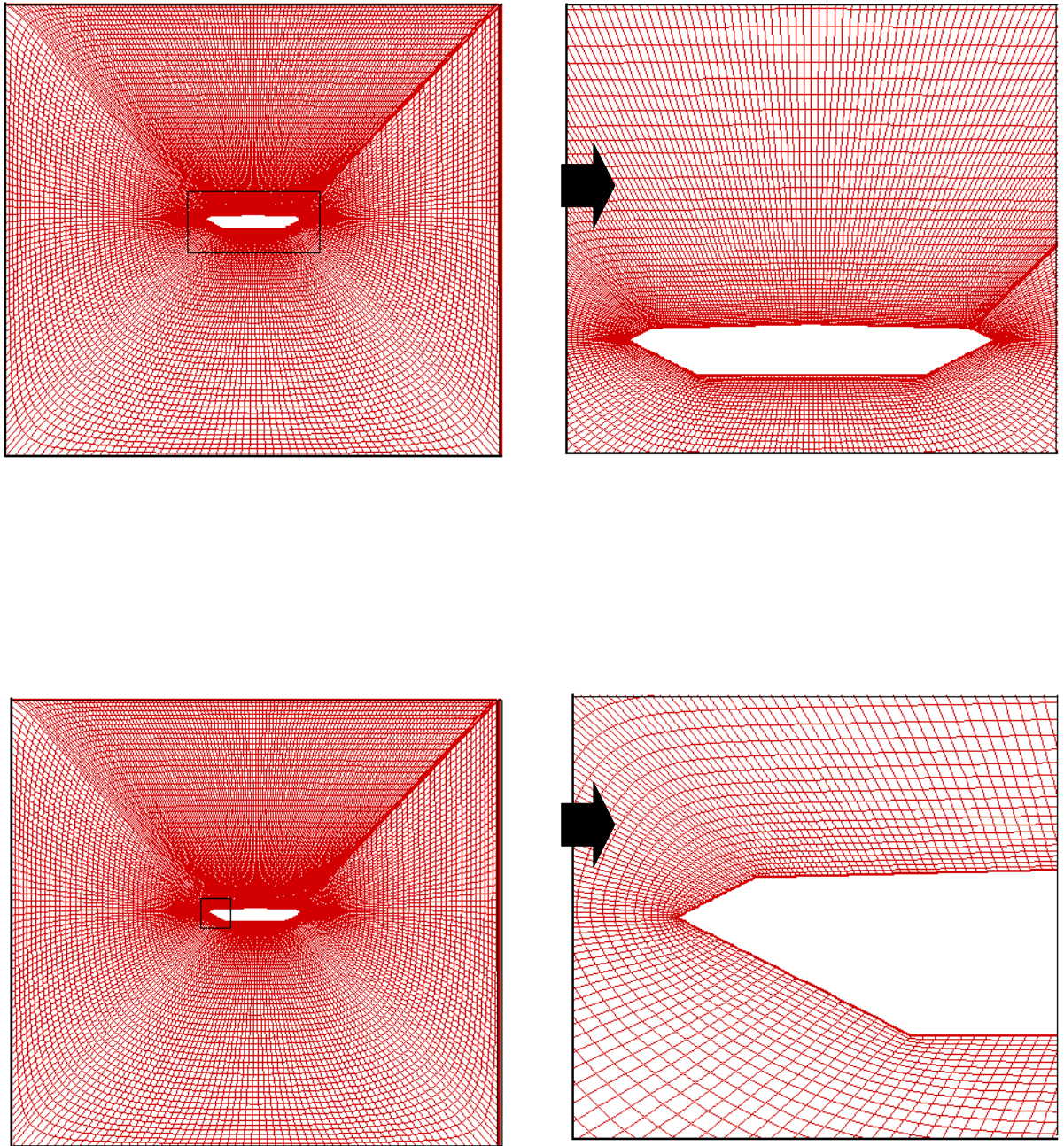


Fig 4.14 Close-up view of Grid-C